Double excitations in correlated systems: A many–body approach

Cite as: J. Chem. Phys. **134**, 034115 (2011); https://doi.org/10.1063/1.3518705
Submitted: 20 August 2010 . Accepted: 01 November 2010 . Published Online: 20 January 2011

Davide Sangalli, Pina Romaniello, Giovanni Onida, and Andrea Marini

Double excitations in correlated systems: A many–body approach

Davide Sangalli,[1,2,3] Pina Romaniello,[3,4,a)] Giovanni Onida,[1,2,3] and Andrea Marini[3,5,6,7]
[1]*Consorzio Nazionale Interuniversitario per le Scienze dei Materiali (CNISM), via della Vasca Navale 84, I-00146 Roma, Italy*
[2]*Dipartimento di Fisica dell' Universitá di Milano, via Celoria 16, I-20133 Milano, Italy*
[3]*European Theoretical Spectroscopy Facility (ETSF)*
[4]*Laboratoire des Solides Irradiés UMR 7642, CNRS-CEA/DSM, École Polytechnique, F-91128 Palaiseau, France*
[5]*Dipartimento di Fisica dell'Università di Roma "Tor Vergata," via della Ricerca Scientifica, I-00133 Roma, Italy*
[6]*IKERBASQUE, Basque Foundation for Science, E-48011 Bilbao, Spain*
[7]*Nano-Bio Spectroscopy Group, Universidad del País Vasco, E-20018 San Sebastián, Spain*

(Received 20 August 2010; accepted 1 November 2010; published online 20 January 2011)

A coherent approach to the description of double excitations in correlated materials is presented: We derive stringent mathematical conditions on the algebraical structure of the Bethe–Salpeter and time-dependent density functional theory kernels that avoid the occurrence of spurious and nonphysical excitations. We discuss how these conditions need to be respected at any level of approximation, including the commonly used local density and static screening approximations. We propose a correlated kernel for the Bethe–Salpeter equation, and we illustrate several aspects of our approach with numerical calculations for model molecular systems. © *2011 American Institute of Physics*. [doi:10.1063/1.3518705]

I. INTRODUCTION

The description of optical absorption spectrum of extended crystalline materials as well as of nano-structured systems is one of the main goals of modern theoretical spectroscopy. In a simplified picture photons are absorbed and turned into electron–hole pairs. It is well-known, however, that in realistic materials the strong spatial localization may lead to the simultaneous formation of two e–h pairs, i.e., double excitations. Double excitations can become essential for the description of the optically excited states in open-shell molecules;[1] however they can play an important role also in closed-shell systems, such as, e.g., in polyenes, where the lowest-lying singlet state is known to have a HOMO^2–LUMO^2 double-excitation character.[2] The theoretical description of double excitations in conjugated polymers constitutes an important challenge for the state-of-the-art approaches used in physics and physical chemistry. Correlation effects, indeed, tend to complicate dramatically the theoretical description and, for this reason, are often neglected. Indeed the most common and widely used approach to the problem of double excitations is given by post-HF methods based on the assumption that correlation is small. However, while this is often reasonable for small molecules, in long 1D molecular chains the effects of correlation are crucial.[3] On the other hand, the currently used approximations to electron correlation in the state-of-the-art approaches to the description of optical excitations in correlated systems, namely time-dependent density functional theory (TDDFT) and many-body perturbation theory (MBPT), fail to capture the physics of double excitations.[1,2]

As post-HF methods are designed to work in a small correlation regime, their extension to realistic materials is very demanding, if not practically impossible. In this article, we make a step beyond the state-of-the-art by showing how to properly use the MBPT and TDDFT schemes to tackle the problem of double excitations in correlated materials.

In the TDDFT approach the excitation energies of a system can be obtained from the noninteracting Kohn–Sham (KS) eigen-energies solving a Dyson equation for the response function. In this equation exchange and correlation (xc) effects are cast in an unknown xc kernel $f_{\mathrm{xc}}[\rho](r, r', t - t') = \delta v_{\mathrm{xc}}[\rho](r, t)/\delta\rho(r', t')$, which needs to be approximated. Most of the success of the TDDFT is due to the success of the adiabatic local density approximation (ALDA), which, despite being extremely simple, is surprisingly accurate in the case of isolated systems. Nevertheless the ALDA suffers from some deficiencies that cause TDDFT to fail in some cases, such as in the description of excited states with a multiple excitation character. The source of this failure has been traced back in the literature to the adiabatic approximation,[1,4] which neglects the frequency dependence of the true xc kernel: It turns out that it is precisely this frequency dependence of the kernel that takes into account all the many-excitation effects.

In MBPT the neutral excitations of the system are obtained by solving the Bethe–Salpeter equation (BSE), which is a Dyson-like equation for a four-point generalized response function. Similarly to TDDFT, xc effects in the BSE are cast in a four-point kernel, which, unlike in TDDFT, can be written as a perturbative expansion. The most common and widely used approximation to this kernel is based on the so-called GW approximation to the self energy, which takes into account the many-body effects acting on a bare particle. Within

a)Present address: Laboratoire de Physique Théorique-IRSAMC, CNRS, Université Paul Sabatier, F-31062 Toulouse Cédex, France.

this approximation the xc effects in the BSE are described by the screened Coulomb interaction W (in the following we will refer to this approximation to the BSE as GW-BSE), which, moreover, is usually considered static, thus ruling out the possibility of describing double excitations.

In the TDDFT literature several solutions to the double excitation problem have been proposed.[1,4–6] Wang and Zeigler used a noncollinear representation of the xc kernel,[6] which could be used to describe double excitations, but only starting from the appropriate reference excited states. Casida proposed a xc kernel which goes beyond the adiabatic approximation constructed from a superoperator formalism[1] that contains as a special case the "dressed–TDDFT" recipe derived by Maitra *et al.*[4] The dressed-TDDFT approach however is not predictive since the existence of double excitations must be defined *a priori*. Only very recently Huix-Rotllant and Casida[7] proposed an extension of the dressed TDDFT method, which clarifies the relation between polarization propagator (PP) approach and the BSE method and is presently being tested on an extensive set of molecules.[7] Finally, in a recent work Romaniello *et al.*[8] proposed an xc kernel that goes beyond the adiabatic approximation starting from the BSE kernel and taking advantage of its connection with the TDDFT kernel. Romaniello *et al.* showed that, by simply relaxing the static approximation to the screened Coulomb interaction, double excitations are in fact described; however, together with the desired excitations, nonphysical excitations also appear. The authors interpret these spurious excitations as due to the self screening error embodied in the GW self energy.[8,9]

The state-of-the-art approaches, then, suffer from different types of pathologies. On one side, HF and post-HF methods can only treat small correlation effects and are, in general, designed to describe isolated systems with the idea that the interactions among particles can be treated perturbatively. These approximations are obtained by truncating the perturbative expansion to some finite order but always respecting key principles of quantum mechanics such as quantum statistics and Pauli exclusion principle. On the other side, in the BSE and TDDFT approaches, correlation is treated to all orders of perturbation theory, but the quantum statistics and Pauli exclusion principle are easily broken in simple approximations, thus leading to uncontrolled effects such as unphysical excitations.

In this paper we propose a novel approach to describe double excitations in correlated materials by embodying the mathematical properties of post-HF methods in a coherent many-body framework. In order to achieve this we first define the conditions for a number-conserving (NC) approach, which avoids the appearance of spurious excitations; we then embody the NC condition in an extension to the BSE that describes double excitations in a consistent manner. The formulation by Romaniello *et al.* is recovered as a subset of the Feynman diagrams included in the present approach, which makes possible to tackle the problem of double excitations in correlated systems.

The paper is organized as follows: In Sec. II we briefly review the second-RPA (sRPA) method, a post-HF approach to the description of double excitations. In particular we discuss the symmetry structure of the sRPA equations, in order to define the conditions that a kernel must fulfill to be number-conserving, i.e., without spurious solutions. The dynamical BSE (DBSE) is introduced in Sec. III, and used in Sec. III C to derive a NC and frequency-dependent kernel. In Sec. IV we report calculations of the polarizability of two hydrocarbon chains, C_8H_2 and C_4H_6, and we show how our approach can produce the correct number of physical excitations, underlying the role played by the various Feynman diagrams. We finally draw our conclusions.

II. THE SECOND RPA: A NUMBER-CONSERVING APPROACH

In the second RPA the equation of motion for the excitation operator (which creates a one-photon state) is solved in the space of single and double excitations. Thus double excitations are explicitly introduced in the formulation. The key concept introduced by the sRPA method that is relevant to our development is the folding of the sRPA equation in the subspace of single excitations.

Both the sRPA and the BSE equation can be cast in the form of an eigenvalue problem. Both approaches in practice describe a generalized response function χ, written in the space of the electron–hole transitions (eh):

$$\chi_{eh,e'h'}(\omega) = \sum_{\lambda\lambda'} \frac{A_{\lambda,eh} S^{-1}_{\lambda\lambda'} A^*_{\lambda,e'h'}}{\omega - E_\lambda}. \tag{1}$$

Here $A_{\lambda,eh}$ and E_λ are, respectively, eigenvectors and eigenvalues of the Hamiltonian associated to the equation of motion for the excitation operator, and $S_{\lambda,\lambda'} = \sum_{eh,e'h'} A^*_{\lambda,eh} A_{\lambda',e'h'}$ is the overlap matrix. The optical response function χ can be easily connected to the macroscopic polarizability tensor by noticing[10] that

$$\overleftrightarrow{\alpha}(\omega) = -\sum_{eh,e'h'} \mathbf{r}_{eh}\ \chi_{eh,e'h'}\ \mathbf{r}_{e'h'}, \tag{2}$$

with $\mathbf{r}_{eh} = \langle e|\mathbf{r}\,|h\rangle$.

A. Second RPA and the folding

The Hamiltonian associated to the sRPA equation of motion can be written[11] in the Fock space of single and double excitations

$$\begin{pmatrix} S & C \\ C^\dagger & D \end{pmatrix} \begin{pmatrix} \mathbf{e}_1 \\ \mathbf{e}_2 \end{pmatrix} = \omega_I \begin{pmatrix} \mathbf{e}_1 \\ \mathbf{e}_2 \end{pmatrix}. \tag{3}$$

Here S and D represent, respectively, the Hamiltonian in the space of single excitations (dimension $N_s \times N_s$) and of double excitations (dimension $N_d \times N_d$). C represents the coupling between single and double excitations. The number of eigenvalues of Eq. (3) is thus, $N_s + N_d$. $\mathbf{e}_1$ and $\mathbf{e}_2$ are the sRPA excitation operator components[11] in the singles and doubles subspaces, respectively.

The question now is how to obtain these N_d poles working only in the space of single excitations, without introducing explicitly the doubles subspace. This step is crucial to create a link between the sRPA and the BSE, which is strictly defined

only in the singles subspace. To create this link we fold the total Hamiltonian matrix in the R^{N_s} subspace.[11] This is done by expressing $\mathbf{e}_2$ in terms of $\mathbf{e}_1$, and then solving the equation for $\mathbf{e}_1$:

$$(S + \Xi(\omega))\,\mathbf{e}_1 = \omega_I \mathbf{e}_1, \tag{4}$$

with $\Xi(\omega) = C(\omega_I - D)^{-1}C^\dagger$. Equations (3) and (4), then, have the same $N_s + N_d$ eigenvalues but Eq. (4) is solved in the single-excitation subspace, and the frequency-dependent kernel $\Xi(\omega)$ takes into account the down-folding of the double-excitation space to the single-excitation space. The correct structure of the Ξ kernel is thus crucial to get the correct number of solutions. In particular, if D can be diagonalized, then Eq. (4) can be written in terms of the diagonal matrix $D' = U^\dagger D U$ as:

$$\left(S + \sum_{\xi=1}^{N_d} \frac{K^{(\xi)}}{(\omega_I - D'_{\xi\xi})}\right)\mathbf{e}_1 = \omega_I \mathbf{e}_1, \tag{5}$$

with $K = C'C'^\dagger$ and $C' = CU$.

An explicit expression for the Ξ kernel of sRPA in the electron–hole and hole–electron transition space (ij) can be found within the Tamm–Dancoff approximation (TDA):[11]

$$\Xi_{(ij),(hk)}(\omega) = \sum_{(nq)(mp)} \frac{C_{(ij),(nq)(mp)}C^\dagger_{(nq)(mp),(hk)}}{\omega - (\epsilon_n - \epsilon_q + \epsilon_m - \epsilon_p)}, \tag{6}$$

with

$$C_{(ij),(nq)(mp)} = \frac{1}{2}(v_{(in),(mp)}\delta_{j,q} + v_{(jq),(mp)}\delta_{i,n} - \{n \leftrightarrow m\} - \{q \leftrightarrow p\} + \{(nq) \leftrightarrow (mp)\}). \tag{7}$$

Here ϵ_i are the poles of the HF Green's function, (GF) G_{HF}, whereas

$$v_{(ij),(hk)} = \int dx dx' \phi^*_j(x)\phi_i(x)v(x,x')\phi_k(x')\phi^*_h(x'), \tag{8}$$

are the projections of the Coulomb interaction in the space of single particle wave functions. The structure of Eq. (6) is the same of the kernel in Eq. (5). A key property of the Ξ kernel is that it remains unchanged under $-\{n \leftrightarrow m\}, -\{q \leftrightarrow p\}$ (Pauli exclusion principle) and $\{(nq) \leftrightarrow (mp)\}$ (particle indistinguishability) transformations, due to the symmetry of the $C_{(ij),(nq)(mp)}$ factors.

Therefore the algebraic structure of Eq. (6) ensures the respect of the particle indistinguishability and of the Pauli exclusion principle which constitute necessary conditions for a number-conserving (NC) theory of double excitations.

This can be shown in detail by solving the characteristic equation arising from Eq. (4), i.e., $\det(\omega - S - \Xi(\omega)) = 0$. Using the nonlinearity of the determinant,

$$\det\left(\frac{K^{(\xi)}}{\omega - D'_{\xi\xi}}\right) = \frac{\det(K^{(\xi)})}{(\omega - D'_{\xi\xi})^{N_s}}$$

(here N_s is the dimension of the matrix K and ξ stands for the set of indexes $\{(nq)(mp)\}$), and exploiting the relation[12] $\det(A + B) = \sum_{P_R,P_C} \mathrm{minor}(A)\,\mathrm{minor}(B)$, (here P_R and P_C are partitions of the rows and the columns of A and B[13]), the eigenvalue equation can then be rewritten as

$$\begin{aligned}&\det(\omega - S - \Xi(\omega))\\ &= \sum_{P_R,P_C} \mathrm{minor}(\omega - S)\,\mathrm{minor}(\Xi(\omega))\\ &= \det(\omega - S) + \sum_{\xi=1}^{N_d} \frac{\det(K^{(\xi)})}{(\omega - D'_{\xi\xi})^{N_s}} + \cdots.\end{aligned} \tag{9}$$

In the last line of Eq. (9) we considered the two terms in the minor expansion that have the maximum and the minimum degree in ω, respectively N_s and $-N_s$. Thus, assuming a completely general structure for the $K^{(\xi)}$ terms, Eq. (9) is a polynomial equation of degree $N_s + N_d N_s$. Consequently the introduction of a frequency-dependent kernel yields, in general, more solutions than the single electron transitions (N_s), although *larger* than the correct number of poles, $N_s + N_d$. However, in our case, the particular structure of the matrices $K^{(\xi)}_{ij,hk} = C_{ij,\xi}C^*_{hk,\xi}$ ensures that *the determinant of any but the one-dimensional sub-block of $K^{(i)}$ is zero*. This means that the second term on the right-hand side (rhs) of Eq. (9) is zero and in the minor expansion only N_d terms of degree -1 survives, from which it follows that the total degree of the polynomial expression $\det(\omega - S - \Xi(\omega))$ is $N_s + N_d$.

In the notation of Eq. (1) $\mathbf{e}_1 = A_{\lambda,eh}$. By plugging the eigenvectors and eigenvalues of Eq. (4) in Eq. (1), we see immediately that the N_d double excitations will appear as poles of $\overleftrightarrow{\alpha}(\omega)$.

B. Second RPA, correlation, and TDA: A closed end

In extended systems the dressing up of bare particles induced by correlation effects is mediated by collective charge oscillations, i.e., by plasmons. Therefore a coherent approach to double excitations in correlated materials should correctly describe the interaction with plasmons. The key problem in the description of plasmons is the possible breakdown of the TDA, as it occurs, for example, in nanostructures.[14] Indeed, within the TDA neutral excitations are described as packets of electron–hole pairs propagating only forward in time, and, therefore, charge oscillations (plasmons) cannot be captured.

sRPA can, in principle, describe plasmons by going beyond the TDA. However, as a matter of fact, the complexity of the method imposes to retain only a few terms beyond TDA. Indeed, the sRPA, given by Eq. (4), is equivalent to a Dyson equation for the response function that can be analyzed by using the diagrammatic technique.

It results that while kernel diagrams [see Fig. 1(a)] are included in the sRPA, self-energy diagrams [see Fig. 1(b)] are not. A more accurate diagrammatic analysis of the sRPA method will be presented in Sec. III C. It has been shown that, starting from the HF approach, including only the kernel diagrams yields an incorrect description of the excitation energies.[15] In a recent paper by Gambacurta *et al.*,[16] studying the spectrum of Sodium clusters, this problem is discussed and identified as lack of ground-state correlation.

This is one of the major reasons why the sRPA approach is not very popular in the condensed matter field.

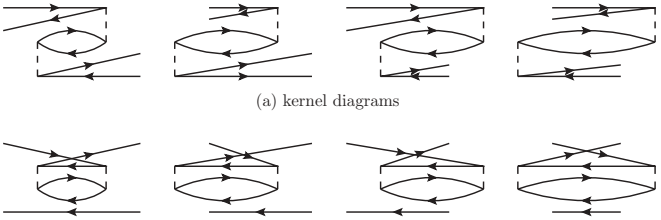

(a) kernel diagrams

(b) self-energy diagrams

FIG. 1. Second-order Feynman diagrams relevant to the description of collective excitations. Time flows from left to right. While kernel diagrams (a) are included in the sRPA, trough the iteration of the Dyson equation, self-energy ones (b) are not. This inconsistency prevent the sRPA to work in a correlated regime.

Approaches like the algebraic diagrammatic construction (ADC) are preferred.[17] However in the ADC approach kernel and self-energy diagrams beyond TDA are included only up to finite orders. While this is a reasonable approach for small systems, it is expected to fail in extended correlated ones. In extended systems, any order diagram in the bare interaction is relevant and kernel and self-energy diagrams must be included up to an infinite order.

III. A NUMBER-CONSERVING APPROXIMATION FOR THE BSE

It is now clear that a well-defined approach to the description of double excitations must be NC, i.e., it must not introduce spurious nonphysical solutions. At the same time, it must include diagrams up to infinite order and beyond the TDA in order to describe screening effect and collective excitations. The BSE approach is an alternative scheme which includes the infinite series of both kernel- and self-energy diagrams, thus providing a suitable approach to achieve both goals in a coherent manner.

A. From the static to the dynamical BSE

The low energy neutral excitations of a N-particle system can be obtained within many body perturbation theory using the BSE,[18]

$$L(12;1',2') = L_0(12;1'2') + L_0(14;1'3)\Xi(35;46)L(62;52'). \quad (10)$$

The variables appearing in the above equations comprise position, spin, and time coordinates: $(1) = (x_1 t_1) = (\mathbf{r}_1 \sigma_1 t_1)$. For simplicity, in the following the spatial and spin dependence will not be specified, if not necessary. Repeated indexes are integrated, as assumed implicitly throughout the paper. L_0 is given in terms of one-particle GFs as $L_0(12;1'2') = -iG(12')G(21')$ and the four-point kernel $\Xi(35;46)$ is given by

$$\Xi(35;46) = i\frac{\delta\left[v_H(3)\delta(34) + \delta\Sigma(34)\right]}{\delta G(65)}, \quad (11)$$

with $v_H(1) = -iv(13)G(33^+)$ the Hartree potential. Physically the two terms on the rhs of Eq. (11) represent exchange interaction (first term) and screening processes (second term) produced by the correlated motion of the electron density.

The optical excitations are obtained in the limiting case $t_1' = t_1, t_2' = t_2$. As a consequence they are given by the poles of $\tilde{L}(\omega) = \int d\omega' d\omega'' L(\omega, \omega', \omega'')$ by considering the Fourier transform of Eq. (10) and using the convention[8,18]

$$L(\omega,\omega',\omega'') = \int d\tau d\tau' d\tau'' e^{i\omega\tau} e^{i\omega'\tau'} e^{i\omega''\tau''} L(t_1, t_1', t_2, t_2'), \quad (12)$$

with $\tau = (t_1 + t_1')/2 - (t_2 + t_2')/2$, $\tau' = t_1 - t_1'$ and $\tau' = t_2 - t_2'$. The BSE then reads:

$$\tilde{L}(\omega) = \tilde{L}_0(\omega) + \frac{1}{4\pi^2}\int d\omega' d\omega'' L_0(\omega,\omega') \times \Xi(\omega,\omega',\omega'')L(\omega,\omega''). \quad (13)$$

Note that Eq. (13) is not a closed equation as the rhs is not a functional of $\tilde{L}(\omega)$. Therefore one usually uses specific approximations to reduce its complexity. The most widely used is based on the GW approximation to the self energy. In this case, the exchange-correlation part of the kernel is approximated as $\partial\Sigma/\partial G \simeq W$ (where the functional derivative $\delta W/\delta G$ is neglected). Furthermore, the energy dependence of W is usually neglected.[19] However, it is now well understood that the resulting static BSE cannot describe double excitations. In Ref. 8 for example, the frequency dependence of $W(\omega)$ has been used to describe double excitations in confined materials. The problem is, that the simple use of a frequency-dependent interaction leads to the appearance of unphysical excitations, as previously mentioned.[8] To trace back those spurious solutions to the kind of diagrams included in the BSE we introduce the dynamical BSE (DBSE),[19] which is obtained by fully exploiting the frequency dependence of Eq. (13). As shown in the Appendix, Eq. (13) can be rewritten as

$$\tilde{L}(\omega) = \tilde{L}_s(\omega) + \tilde{L}_s(\omega)\Xi^d(\omega)\tilde{L}(\omega). \quad (14)$$

In Eq. (14) $\tilde{L}_s(\omega) = -iG_sG_s$ with G_s the one-particle GFs containing the static part only of the self energy; Ξ^d is composed of the two terms, Ξ_1^d and Ξ_2^d: Ξ_1^d describes the contributions coming from the dynamical part of the self energy (its derivation is outlined in the Appendix); Ξ_2^d describes the contributions coming from the electron–hole coupling and is obtained by multiplying the second term of the rhs of Eq. (13) by $\tilde{L}_0(\omega)\tilde{L}_0^{-1}(\omega)$ on the left and by $\tilde{L}^{-1}(\omega)\tilde{L}(\omega)$ on the right,

$$\Xi_1^d(\omega) \simeq -i\tilde{L}_s^{-1}(\omega)\int\frac{d\omega'}{2\pi}\big[G_s(\omega'+\omega/2)G_s(\omega'-\omega/2) \times \Sigma_d(\omega'-\omega/2)G(\omega'-\omega/2) + G_s(\omega'+\omega/2) \times \Sigma_d(\omega'+\omega/2)G(\omega'+\omega/2)G_s(\omega'-\omega/2)\big], \quad (15)$$

$$\Xi_2^d(\omega) = \tilde{L}_0^{-1}(\omega)\frac{1}{(2\pi)^3}\int d\omega' d\omega'' d\omega''' L_0(\omega,\omega',\omega'') \times \Xi(\omega,\omega',\omega''')L(\omega,\omega''',\omega'')\tilde{L}^{-1}(\omega). \quad (16)$$

The complexity of the original Eq. (13) is thus transferred, in Eq. (14), in the structure of the DBSE kernel $\Xi_d(\omega)$. We can, however, simplify the dependence on G and L in $\Xi_d(\omega)$

by starting from its linear limit where $G(\omega) \simeq G_s(\omega)$ in Eq. (15) and $L(\omega, \omega', \omega'') \simeq L_0(\omega, \omega', \omega'') \simeq L_s(\omega, \omega', \omega'')$ in Eq. (16). This limit is fully justified in the DBSE by the fact that, as shown in the following, it accounts for the simultaneous evolution of two e–h pairs, which represent the dominant channel in the description of double excitations.

We need now to approximate the unknown quantities Σ_s, $\Sigma_d(\omega)$ and $\Xi(\omega, \omega', \omega'')$. For the static part of the self energy we consider the common $\Sigma = iGW$ approximation evaluated at the quasi-particle eigen-energies. The dynamical part of the self energy $\Sigma_d(\omega)$ and the kernel $\Xi(\omega, \omega', \omega'')$ are derived later in the paper: Starting from the sRPA approach we obtain a kernel Ξ^d that fulfills the NC condition and that includes the statically screened Coulomb interaction in the $\omega \to 0$ limit, thus recovering the commonly used static *GW*-BSE.

B. DBSE in the configuration space

The DBSE can be solved by projecting Eq. (14) in the basis of single particle wave functions $\{\psi_i\}$,

$$\tilde{L}_{(ij)(hk)}(\omega) = \int d^3\mathbf{x}_1 d^3\mathbf{x}_2 d^3\mathbf{x}_3 d^3\mathbf{x}_4 \; \phi_i(\mathbf{x}_1)\phi_j^*(\mathbf{x}_2) \times \tilde{L}(\mathbf{x}_1\mathbf{x}_2; x_3\mathbf{x}_4; \omega)\phi_h^*(\mathbf{x}_3)\phi_k(\mathbf{x}_4). \quad (17)$$

The indexes (ij) represent hole–electron and electron–hole pairs, as in Eq. (6). Eq. (14) can then be recast in the form of an eigenvalue problem,

$$\begin{pmatrix} H(E_\lambda) & K(E_\lambda) \\ -K^*(-E_\lambda) & -H^*(-E_\lambda) \end{pmatrix} (A_{\lambda,ij}(E_\lambda)) = E_\lambda(A_{\lambda,ij}(E_\lambda)), \quad (18)$$

where

$$H_{(ij)(hk)}(\omega) = \delta_{i,h}\delta_{j,k}(\epsilon_j - \epsilon_i) + \Xi^d_{(ij)(hk)}(\omega), \quad (19)$$

$$K_{(ij)(hk)}(\omega) = \Xi^d_{(ij)(kh)}(\omega). \quad (20)$$

Here ϵ_i are the poles of the one-particle GF and E_λ are the excitation energies of the system. Eigenvectors and eigenvalues of Eq. (18) can be used to evaluate $\overleftrightarrow{\alpha}(\omega)$ as shown in Eq. (1). Using a static approximation for the kernel, the K and H sub-blocks become ω independent and consequently the number of eigenvalues of Eq. (18) is strictly equal to the dimension of the matrix, that is the number of single-particle transitions N_s. Double excitations are then not described at all. Instead, by retaining the full frequency dependence of the DBSE kernel Eq. (18) becomes a nonlinear equation whose solutions, in general, are more than N_s. This gives us a close connection with the sRPA equations and the ideal starting point for imposing the NC condition to the DBSE kernel.

C. A number-conserving kernel for the BSE

The DBSE equation provides a powerful starting point to tackle the double-excitation problem, as the diagrammatic approach makes possible to introduce different levels of approximation that overcome the limits of the sRPA. We achieve this by following two essential steps: (i) we use the sRPA to establish a connection between Feynmann diagrams and particle indistinguishability and the Pauli exclusion principle; (ii) we use this connection to define a number-conserving correlated kernel starting from the well established *GW* approximation.

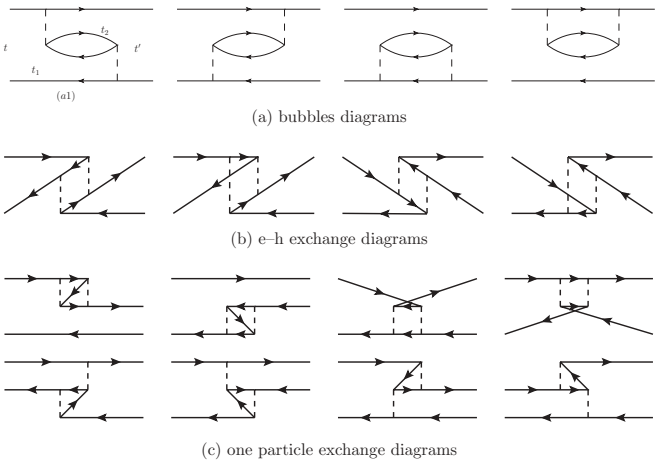

FIG. 2. Basic Feynman diagrams included in the second RPA approach (Ref. 11) beyond the standard TDHF. The time flows from left to right respecting the Tamm–Dancoff approximation. The sRPA approach, when the TDA is relaxed, includes other 16 basic diagrams obtained by inverting the direction of all *GF*. The complete set of diagrams is obtained by iterating the Dyson equation.

1. The diagrammatic number conserving rule

In order to create a common language for both the sRPA and the DBSE approaches, we start by noticing that within the TDA, sRPA is equivalent to the DBSE when $\Sigma_s = \Sigma_{\mathrm{HF}}$. Specifically, $\Sigma_d(\omega)$ contains all second-order Feynman diagrams, and $\Xi(\omega) = [\partial(\Sigma_s + \Sigma_d)]/\partial G$. The 16 diagrams of Fig. 2, in particular, come from Σ_d and its functional derivative. From now on we work within TDA, in order to keep the discussion as simple as possible.

To understand why double excitations are described within this approximation we focus on diagram (a1) in Fig. 2(a), drawn for a specific time ordering. The diagram describes a physical process where the electron–hole pair created at time t emits a photon that generates another electron–hole pair at time t_1. The second e–h pair is annihilated at time t_2. Therefore this Feynman diagram is describing the coupling between a single and a double excitation.

By taking into account the 16 diagrams of Fig. 2, the DBSE (and consequently the sRPA) correctly describes *particle indistinguishability* and *Pauli exclusion principle*. Here we illustrate how this can be deduced from the inspection of Feynman diagrams. The 16 diagrams describe processes in which a double excitation appears from a photon emitted either from the electron or from the hole and then absorbed back [these two possibilities are the first two terms in the definition of $C_{(ij),(nq)(mp)}$, see Eq. (7)]. Therefore each double-excitation process can start and end in two ways so that there are four possible processes, which are the four bubble diagrams of Fig. 2. The other 12 diagrams reflect the particle indistinguishability that imposes the electron lines, as well as the hole lines, to be interchangeable between each other. Following

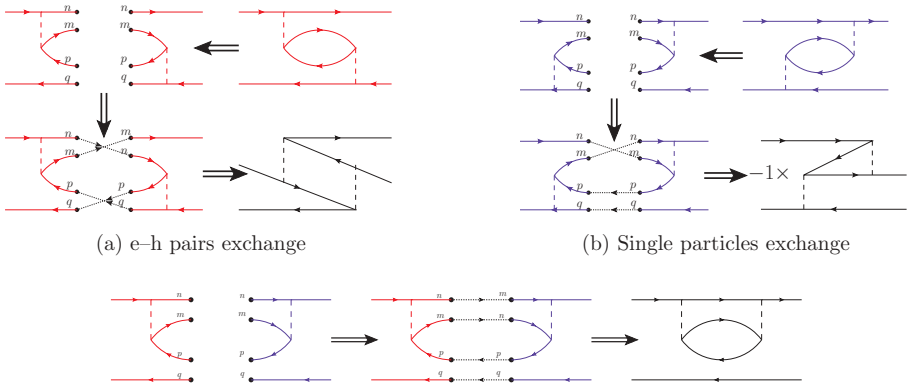

(a) e–h pairs exchange (b) Single particles exchange

(c) Half diagrams recombination

FIG. 3. The DNCR in practice. We take as reference the two time orderings of the kernel bubble diagram, corresponding to the two first diagrams of Fig. 2. The general procedure to get a NC kernel is to split each initial diagram in two half diagrams. Then these half diagrams must be connected by exchanging in all possible ways all e–h pairs and all single particles. This produces a new group of diagrams that must be processed using the same procedure. When no new diagrams appear the resulting kernel is NC.

Fig. 3 we can derive a graphical rule that any approximation has to respect in order to be NC, this is the proposed diagrammatic number conserving rule (DNCR). First we consider an initial group of diagrams, chosen in such a way to describe the relevant physics we want to introduce in the theory (like plasmons and excitons). Then we split any diagram in two parts that, connected in all possible ways obtained by imposing particle exchange, lead to a new group of diagrams. When the same procedure applied to the resulting diagrams does not lead to any new diagram the approximation is, by definition, NC. As an illustration, the DNCR can be applied to the sRPA diagrams, shown in Fig. 2. It can be shown that *all* sRPA diagrams can be obtained from the first two by applying the proposed DNCR.

2. The DNCR applied to the BSE

A crucial consequence of the DNCR is that, as exemplified in Fig. 3, a NC kernel must include all kinds of diagrams. Therefore, whatever initial approximation is chosen, the repeated application of the DNCR will create a balanced mixture of diagrams in order to respect particle indistinguishability and Pauli exclusion principle. If the DNCR is not respected by selecting only a class of diagrams, then spurious solutions are expected to appear. This is the case of the kernel proposed in Ref. 8, which was obtained from the standard $\Xi \simeq W(\omega)$ by simply relaxing the static approximation for W. This kernel introduces an infinite series of RPA diagrams only in the interaction W, neglecting all consequent diagrams imposed by the DNCR. As a consequence spurious poles in the polarizability are found as predicted by the DNCR.

Nevertheless the kernel proposed in Ref. 8 describes the interaction with plasmons, which is a desirable property we want to retain, at the same time forcing the kernel to be NC. However, before applying the DNRC, we have to notice that the $W(\omega)$ propagator describes the evolution of charge oscillations, composed by renormalized packets of e–h pairs. This clearly introduces a distinction between the e–h pairs embodied in $W(\omega)$ and the real e–h pairs created by the scattering process, thus leading to the breakdown of particle indistinguishability. A better starting point is instead the basic diagram shown in Fig. 4, where all e–h pairs are correctly renormalized. In this diagram the filled bubble and the filled rectangle represent the RPA response function $\chi^{\mathrm{RPA}}(\omega)$. By introducing the Lehman representation for χ^{RPA} we can write

$$\chi^{\mathrm{RPA}}_{eh,e'h'}(\omega) = \sum_{\nu} \frac{R_{\nu,eh} R^{*}_{\nu,e'h'}}{\omega - \Omega_{\nu}}. \tag{21}$$

Here $R_{\nu,eh}$ and Ω_{ν} can be obtained as solution of the time-dependent Hartree equation written in the e–h basis. We will call the poles of χ^{RPA} RPA excitations. Notice that in the long-wavelength limit these excitations describe the plasmonic oscillations.

The DNCR imposes to consider all possible diagrams obtained from Fig. 4 by exchanging the basic excitation propagators. The key point here is to rotate from the independent e–h pairs to the RPA basis, where e–h pairs are replaced by the RPA excitations. Therefore we proceed by splitting the RPA propagators, using Eq. (21), as sketched in Fig. 5. Then we consider all diagrams where the RPA excitations are exchanged.

Mathematically the procedure sketched in Fig. 5 corresponds to rotate in the RPA excitation space the residuals and poles of Eq. (6). Each term in the rotated counterpart of Eq. (7) will correspond to a possible connection induced by

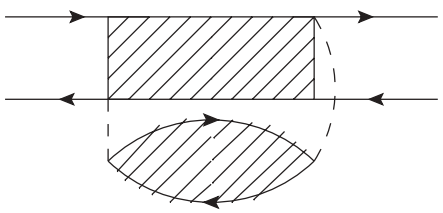

FIG. 4. Basic RPA diagram used as a starting point for the correlated kernel. All other diagrams are obtained by applying the DNCR, as discussed in the text.

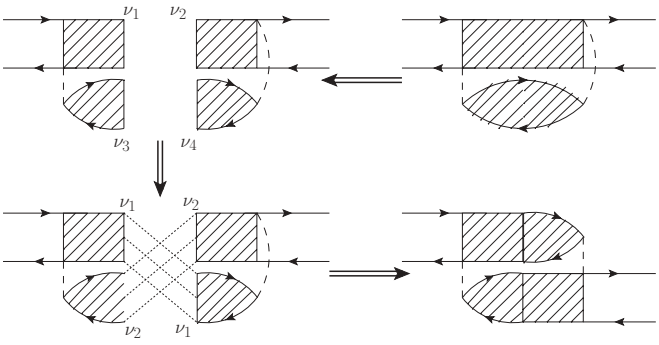

FIG. 5. Building up of correlated Feynman diagrams connecting two Feynman diagrams. The effect of exchange among two RPA excitations is shown by the dotted lines.

the DNCR:

$$C^{\mathrm{RPA}}_{(ij),\nu_1\nu_2} = \frac{1}{2}\sum_{(nq),(mp)} ((v_{(in),(mp)}\delta_{j,q} + v_{(mp),(jq)}\delta_{i,n}) \times R_{\nu_1,(np)}R_{\nu_2,(mq)} + \{\nu_1 \leftrightarrow \nu_2\}). \quad (22)$$

As a consequence the correlated version of Eq. (6) will look like

$$\left(\Xi^d_{\mathrm{RPA}}\right)_{(ij),(hk)} = \sum_{\nu_1\neq\nu_2} \frac{C^{\mathrm{RPA}}_{(ij),\nu_1\nu_2}\left[C^{\mathrm{RPA}}_{(hk),\nu_1\nu_2}\right]^*}{\omega - (E_{\nu_1} + E_{\nu_2} + 2i\eta)}. \quad (23)$$

The symbol $\{\nu_1 \leftrightarrow \nu_2\}$ in Eq. (22) imposes the invariance of the correlated kernel under exchange of RPA excitations. Consequently the kernel Ξ^d_{RPA} is by definition invariant under exchange of two RPA excitations. However RPA excitations are bosons, so that Pauli exclusion principle does not apply and the obtained kernel is not fully NC. To fix this problem it is sufficient to impose the condition $\nu_1 \neq \nu_2$ in Eq. (23).

The DBSE obtained by using the Ξ^d_{RPA} kernel includes all self-energy terms obtained from $\Sigma_d = GW - \Sigma_s$ and $\Xi(\omega, \omega', \omega'') = \delta(\omega - \omega')W(\omega' - \omega'')$. In addition, extra terms appear in order to fulfill the NC condition. Interestingly Ξ^d_{RPA} also embodies the full-frequency-dependent term $G\,\delta W/\delta G(\omega)$, which is usually neglected in the standard BSE approach. In the present case these second-order diagrams in W are indeed needed to correctly account for the particle indistinguishability. The resulting kernel, whose diagrammatic expression is sketched in Fig. 6, does have the right mathematical structure by construction, so that no spurious solutions are present.

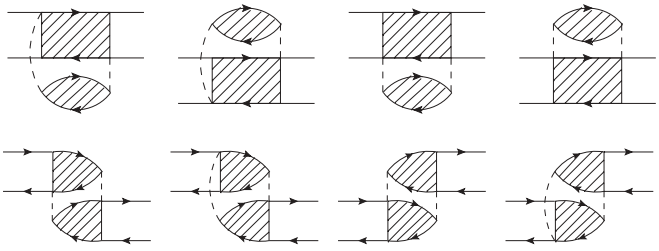

FIG. 6. The final correlated DBSE kernel. The filled regions represent the propagation of RPA excitations.

IV. NUMERICAL RESULTS ON MODEL MOLECULAR SYSTEMS

In the following we will illustrate various conceptual and technical aspects of our approach using two benchmark model systems, based on the C_8H_2 and the C_4H_6 molecules. These unsaturated hydrocarbon chains are often chosen as benchmark systems to test theoretical methods aimed to describe double excitations. By calculating the polarizability of these systems we will show: (i) The role played by subgroups of diagrams in the description of double excitations; (ii) the fact that the number conserving rule not only applies to the total number of poles, but also to the number of optically active poles; (iii) the absence of spurious double excitation peaks that appear in approaches[8] that violate the NC rule.

The calculations have been performed using the YAMBO code,[21] where we implemented sRPA for closed-shell systems, within the TDA. Furthermore we approximate both QP and HF wave functions with KS–LDA wave functions.

sRPA produces results similar to the GW-BSE approach or to the DBSE when only "bubble diagrams" (first row of Fig. 2) or "bubble diagrams and e–h exchange diagrams" (second row of Fig. 2), respectively, are selected. Therefore this implementation allows us to explore the performances of the various approaches by selecting specific subgroups of diagrams.

We first performed a ground-state calculation with the ABINIT code,[22] within DFT/LDA, with an energy plane-wave cutoff of 20 Hartree and a super cell of 25 × 25 × 40 Bohr for the C_8H_2 (a linear molecule ≈ 21 Bohr long) and a smaller super cell of 25 × 25 × 15 Bohr for the C_4H_6 (the molecule extends for ≈10 Bohr both in the x and y directions). Then we performed excited-state calculations in the basis set of KS states, considering only the states from HOMO −3 to LUMO +3. In this way our systems can be mapped into an eight level model with 16 single and 240 double excitations. All the C_8H_2 eigenvalues are doubly degenerate due to the symmetry of the molecule.

In the description of double excitations the kernel frequency dependence becomes crucial when one or more poles fall in the absorption spectrum energy range. In this case the static approximation fails, and extra peaks appear. In order to artificially simulate this situation in our systems we use HF eigenvalues to construct L_0, while the kernel is built with KS–LDA ones. This choice gives us the possibility to investigate more physical situations which could arise for correlated materials.

The results of these calculations are plotted in Fig. 7. For both systems at the HF independent-particle (IP) level there is a clear peak, which falls close to 9 eV for the C_8H_2, and close to 12 eV for C_4H_6. As expected the kernel constructed with KS–LDA eigenvalues has poles in these energy ranges, so that extra peaks appear in the spectrum. The effect is visible in both model systems: in C_8H_2 the main peak is essentially split in two [see Fig. 7(a)]; for C_4H_6 several extra peaks appear as shown in the inset of Fig. 7(b).

We will now explore the role played by the various subgroups of diagrams, namely (a) the bubble diagrams in

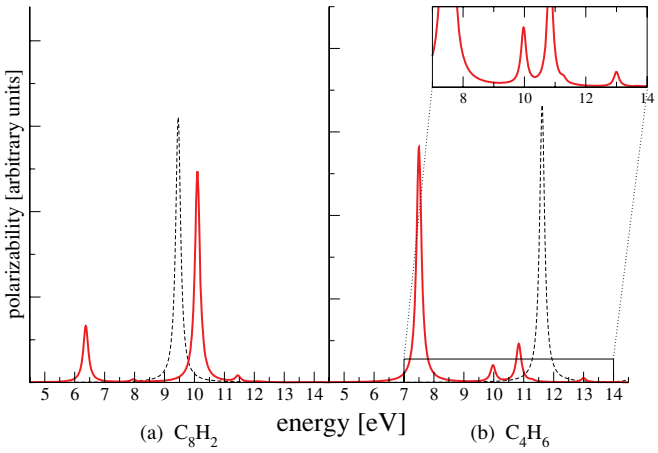

FIG. 7. Second random phase approximation spectra. For both model systems the frequency-dependent kernel produces extra peaks (red line) which cannot be described by a static kernel. The black thin dashed line is the independent-particle spectrum. The inset is present here as reference to detect spurious peaks in the insets of Figs. 8 and 9.

Fig. 2(a); (b) the e–h exchange diagrams in Fig. 2(b), which are obtained from the bubble diagrams via e–h exchange; (c) the particle exchange diagrams in Fig. 2(c), which are obtained from the bubble diagrams via single-particle exchange.

Figure 8 shows the spectra obtained taking into account, beyond the TDHF scheme, only selected families of diagrams. By selecting only diagrams of type (b) or (c) the spectra are not positive defined. This unphysical property can be understood by noticing that the frequency-dependent kernel constructed from diagrams (b) and (c) does not have the mathematical structure of Eq. (6). On the contrary, the kernel constructed from the bubble diagrams (a) is positive, though particle indistinguishability and Pauli exclusion principle are not respected as illustrated in previous sections.

Indeed the spectra constructed from bubble diagrams is positive defined, though spurious peaks appear: in C_8H_2 [Fig. 8(a)] one has three peaks at around 12 eV, and in the C_4H_6 many peaks appear [see Fig. 8(b), the left inset] which are not present in the full sRPA spectra.

Figure 9 shows the spectra constructed taking into account both subsets of diagrams (a) and (b) or (a) and (c) together. The spectra are positive defined. However, only the former combination gives the right number of peaks (i.e., the same number of the full sRPA spectrum) whereas the latter produces spurious poles.

In this perspective, it is interesting to compare the two cases. In the C_8H_2 model the subset of diagrams (a) and (b) (green dashed line) gives a spectrum which is very close to the full sRPA spectrum of Fig. 7 (red line) both in the structure and number of poles. Diagrams of kind (c) are, instead, negligible.

In the C_4H_6 model, on the contrary, diagrams of kind (c) play an important role: They shift the peak of the bubbles polarizability toward the results obtained with the sRPA kernel. Diagrams of kind (b), instead, in this case have a negligible effect on the position of the peaks. However the choice (a) + (c) gives several spurious poles [see Fig. 9(b), blue line in the right inset] and, as for C_8H_2, only the combination (a) and (b) yields the correct number of poles [see Fig. 9(b), green dashed line in the left].

The sum of diagrams (a) and (b) describes e–h pairs as indistinguishable bosons, whereas the sum of diagrams (a) and (c) does not correspond to any defined statistic. We can then conclude that diagrams of kind (c) are meaningful only if added to the other two classes of diagrams in order to describe particle indistinguishability. However, the spectrum obtained combining the diagrams (a) and (b) has indeed the same number of peaks of the spectrum obtained using the complete kernel, thus supporting our recipe to construct a correlated kernel

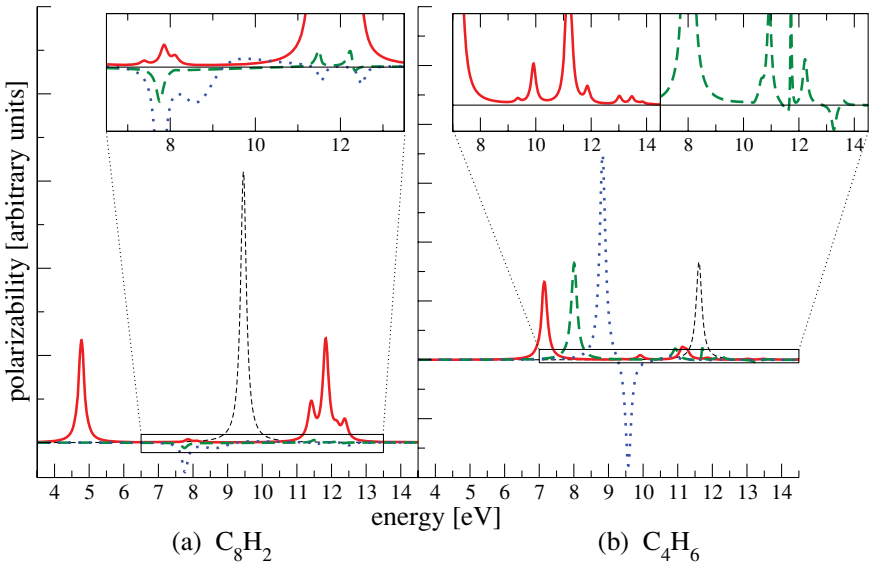

FIG. 8. The spectra obtained selecting only specific subgroup of diagrams. By selecting only e–h exchange (green dashed line) or one particle exchange (blue dots) an unphysical (negative) polarizability is observed. Only the spectra obtained with the kernel constructed using the bubble diagrams (red line) is positive defined. However when only bubble diagrams are used, as proposed by Romaniello *et al.* (Ref. 8), spurious peaks appear. These peaks do not appear in the spectra obtained from the full sRPA kernel (see Fig. 7).

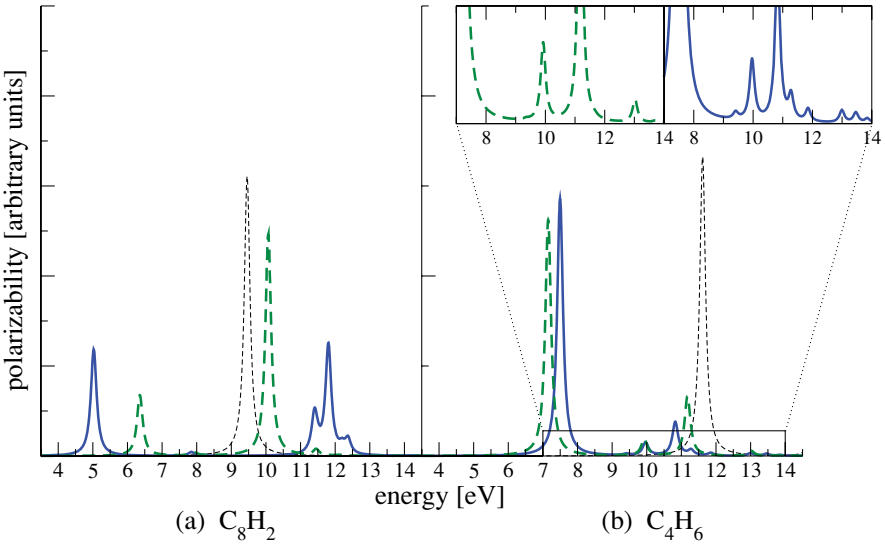

FIG. 9. Spectra obtained with the kernel constructed using the bubble plus e–h exchange diagrams (green dashed line) and the bubble plus e–h exchange diagrams (blue line). Both spectra are positive defined but only the combination bubbles plus e–h exchange gives the same number of poles of the full sRPA spectra (see Fig. 7). On the contrary the combination bubbles plus one particle exchange gives spurious solutions.

discarding the subset of diagrams (c). Another conclusion we draw from these results is that our approach, by respecting the NC rule, ensures that the theory produces not only the correct total number of poles, but also the correct total number of *optically active* (and optically not active) poles.

V. CONCLUSIONS

With the present paper we presented a method to include double excitations in a consistent manner within the GW + BSE approach. The main idea has been to correct the standard BSE kernel in order to go beyond the static approximation while, at the same time, fulfilling the number conserving condition. The resulting scheme keeps all the advantages of the many-body approach, that is the ability of describing extended and correlated materials in a consistent manner, without producing spurious excitations.

We derived a number–conserving condition from an inspection of the similarities and the differences between the BSE scheme, designed for solids, and the sRPA approach, designed for isolated systems. While in the BSE screening plays a crucial role, the sRPA shows the importance of particle exchange effects. As pointed out in a very recent work by Huix-Rotllant and Casida,[7] there is a great interest in this direction in order to develop approximations at the nanoscale interface between molecules and solids. In contrast to previous approaches, however, we do not directly consider all exchange diagrams related to the RPA screening resummation, because we believe that such an approach would be unpractical, especially for realistic materials. Instead, our method is aimed to capture the main feature related to the exchange principle without requiring to diagonalize matrices in the space of double excitations.

Our numerical calculations on model molecular systems show that the bubbles plus e–h exchange Feynman diagrams, chosen as reference for our correlated kernel, are essential to get the correct number of physical excitations. The kernel constructed from these diagrams produces double excitations without any extra spurious peak and the number conserving rule turns out to apply also to the number of optically active poles.

ACKNOWLEDGMENTS

This work was supported by the EU through the FP7 ETSF I3 e-Infrastructure (Grant Agreement 211956). D. Sangalli, G. Onida and P. Romaniello would like to thank Prof. Gianluca Colò for many useful discussions on the sRPA method and on the interpretation of the link between Feynmann diagrams and double excitations. D. Sangalli and G. Onida acknowledge several useful discussions with Miquel Huix-Rotllant and Mark Casida, and thank them for providing us with a preprint of their reference [7] prior to publication. Andrea Marini would like to acknowledge support from the HPC-Europa2 Transnational collaboration project.

APPENDIX: CONTRIBUTION OF THE SELF-ENERGY DIAGRAM TO THE DBSE KERNEL

The self-energy terms in the kernel of the BSE equation are due to the $\tilde{L}_0(\omega) = -i \int d\omega'/(2\pi) G(\omega' + \omega/2) G(\omega' - \omega/2)$ term. We start from the Dyson equation for the Green's Function written in the form:

$$G^{-1} = g^{-1} - \Sigma_s - \Sigma_d(\omega) = G_s^{-1} - \Sigma_d(\omega). \qquad \text{(A1)}$$

where $G_s^{-1} = g^{-1} - \Sigma_s$, and we split the self-energy in its static (Σ_s) and dynamic (Σ_d) parts. We can then write:

$$\begin{aligned}\tilde{L}_0(\omega) &= \tilde{L}_s(\omega) - i\int \frac{d\omega'}{2\pi} G_s(\omega'+\omega/2)G_s(\omega'-\omega/2) \\ &\times \Sigma_d(\omega'-\omega/2)G(\omega'-\omega/2) - i\int \frac{d\omega'}{2\pi} G_s(\omega'+\omega/2) \\ &\times \Sigma_d(\omega'+\omega/2)G(\omega'+\omega/2)G_s(\omega'-\omega/2) \\ &- i\int \frac{d\omega'}{2\pi} G_s(\omega'+\omega/2)\Sigma_d(\omega'+\omega/2)G(\omega'+\omega/2) \\ &\times G_s(\omega'-\omega/2)\Sigma_d(\omega'-\omega/2)G(\omega'-\omega/2), \qquad \text{(A2)}\end{aligned}$$

where $\tilde{L}_s = -iG_sG_s$. Using the same trick adopted for the kernel, we multiply the second, third, and fourth term on the right-hand side of Eq. (A2) by $\tilde{L}_s\tilde{L}_s^{-1}$ from the left and by $\tilde{L}_0^{-1}\tilde{L}_0$ from the right, and we obtain

$$\tilde{L}_0(\omega) = \tilde{L}_s(\omega) + \tilde{L}_s(\omega)\Xi_1^d(\omega)\tilde{L}_0(\omega). \qquad \text{(A3)}$$

Equation (A3) defines the $\Xi_1^d(\omega)$ kernel:

$$\begin{aligned}\Xi_1^d(\omega) = -i\tilde{L}_s^{-1}(\omega)\int \frac{d\omega'}{2\pi}\big[&G_s(\omega'+\omega/2)G_s(\omega'-\omega/2) \\ &\times \Sigma_d(\omega'-\omega/2)G(\omega'-\omega/2) + G_s(\omega'+\omega/2) \\ &\times \Sigma_d(\omega'+\omega/2)G(\omega'+\omega/2)G_s(\omega'-\omega/2) \\ &+ G_s(\omega'+\omega/2)\Sigma_d(\omega'+\omega/2)G(\omega'+\omega/2) \\ &\times G_s(\omega'-\omega/2)\Sigma_d(\omega'-\omega/2)G(\omega'-\omega/2)\big] \\ &\times \tilde{L}_0^{-1}(\omega). \qquad \text{(A4)}\end{aligned}$$

To describe double excitations we will neglect the last term on the rhs of Eq. (A2) as it describes a process where six Green-function lines appear simultaneously, thus inducing a triple excitation. Moreover we linearize the expression for the kernel setting $\tilde{L}_0 \simeq \tilde{L}_s(\omega)$ and $G(\omega) \simeq G_s(\omega)$ as diagrams beyond this approximation describe processes not included within the two-particles two-holes space. Accordingly it is crucial that the static part of the self energy is treated in a separate way. In fact, it has been shown, within the standard GW approximation, that the linearization of the static self-energy contribution is numerically unstable and gives rise to scattered spectra.[20]

[1] M. E. Casida, J. Chem. Phys. **122**, 054111 (2005).
[2] R. J. Cave, F. Zhang, N. T. Maitra, and K. Burke, Chem. Phys. Lett. **389**, 39 (2004).
[3] D. Varsano, A. Marini, and A. Rubio, Phys. Rev. Lett. **101**, 133002 (2008).
[4] N. T. Maitra, F. Zhang, R. J. Cave, and K. Burke, J. Chem. Phys. **120**, 5932 (2004).
[5] C. M. Isborn and X. Li, J. Chem. Phys. **129**, 204107 (2008).
[6] F. Wang and T. Ziegler, J. Chem. Phys. **121**, 12191 (2004).
[7] M. Huix-Rotllant and M. E. Casida, arXiv:1008.1478v1 [cond-mat.mes-hall] 9 Aug 2010. "Formal Foundations of Dressed Time-Dependent Density-Functional Theory for Many-Electron Excitations."
[8] P. Romaniello, D. Sangalli, J. A. Berger, F. Sottile, L. G. Molinari, L. Reining, and G. Onida, J. Chem. Phys. **130**, 044108 (2009).
[9] P. Romaniello, S. Guyot, and L. Reining, J. Chem. Phys. **131**, 154111 (2009).
[10] G. Onida, L. Reining, and A. Rubio, Rev. Mod. Phys. **74**, 601 (2002).
[11] J. Wambach, Rep. Prog. Phys. **51** (1988).
[12] V. E. Korepin, N. M. Bogoliubov, and A. G. Izergin, "Quantum inverse scattering method and correlation functions," in *Cambridge Monographs on Mathematical Physics* (Cambridge University Press, Cambridge, 1997), Appendix IX.1.
[13] By minor(A) we mean the usual definition as the determinant of a submatrix M obtained rasing a fixed number n of columns and rows. The terms $n = 0$, i.e. the determinant of the matrix $M = A$, is considered too.
[14] M. Gruning, A. Marini, and X. Gonze, Nano Lett. **9**, 2820 (2009).
[15] J. Brand and L. S. Cederbaum, Phys. Rev. A **97**, 4311 (1998).
[16] D. Gambacurta and F. Catara, Phys. Rev. B **79**, 085403 (2009).
[17] J. Schirmer, Phys. Rev. A **26**, 2395 (1982).
[18] G. Strinati, Rev. Nuovo Cimento **11**, 1 (1988).
[19] A. Marini and R. Del Sole, Phys. Rev. Lett. **91**, 176402 (2003).
[20] F. Bruneval, F. Sottile, V. Olevano, and L. Reining, J. Chem. Phys. **124**, 144113 (2006).
[21] A. Marini, C. Hogan, M. Grüning and D. Varsano, Comp. Phys. Comm. **180**, 1392 (2009).
[22] X. Gonze, B. Amadon, P.-M. Anglade, J.-M. Beuken, F. Bottin, P. Boulanger, F. Bruneval, D. Caliste, R. Caracas, M. Cote, T. Deutsch, L. Genovese, Ph. Ghosez, M. Giantomassi, S. Goedecker, D. R. Hamann, P. Hermet, F. Jollet, G. Jomard, S. Leroux, M. Mancini, S. Mazevet, M. J. T. Oliveira, G. Onida, Y. Pouillon, T. Rangel, G.-M. Rignanese, D. Sangalli, R. Shaltaf, M. Torrent, M. J. Verstraete, G. Zerah, and J. W. Zwanziger, Comput. Phys. Commun. **180**, 2582 (2009).